

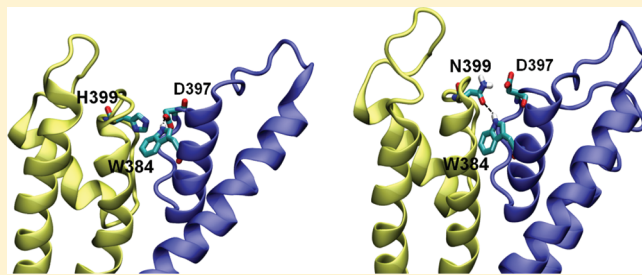
Charybdotoxin and Margatoxin Acting on the Human Voltage-Gated Potassium Channel $hK_v1.3$ and Its H399N Mutant: An Experimental and Computational Comparison

Azadeh Nikouee,^{†,‡} Morteza Khabiri,^{†,§} Stephan Grissmer,^{*,‡} and Rüdiger Ettrich^{*,§}

[†]Institute of Applied Physiology, Ulm University, Albert-Einstein-Allee 11, 89081 Ulm, Germany

[§]Institute of Nanobiology and Structural Biology of GCRC, Academy of Sciences of the Czech Republic, and Faculty of Sciences, University of South Bohemia in Ceske Budejovice, Zamek 136, CZ-373 33 Nove Hrady, Czech Republic

ABSTRACT: The effect of the pore-blocking peptides charybdotoxin and margatoxin, both scorpion toxins, on currents through human voltage-gated $hK_v1.3$ wild-type and $hK_v1.3$ _H399N mutant potassium channels was characterized by the whole-cell patch clamp technique. In the mutant channels, both toxins hardly blocked current through the channels, although they did prevent C-type inactivation by slowing down the current decay during depolarization. Molecular dynamics simulations suggested that the fast current decay in the mutant channel was a consequence of amino acid reorientations behind the selectivity filter and indicated that the rigidity–flexibility in that region played a key role in its interactions with scorpion toxins. A channel with a slightly more flexible selectivity filter region exhibits distinct interactions with scorpion toxins. Our studies suggest that the toxin–channel interactions might partially restore rigidity in the selectivity filter and thereby prevent the structural rearrangements associated with C-type inactivation.



the outer vestibule and/or a collapsed and constricted region in the selectivity filter of the channel,^{19,20} as well as the pore helix and the first part of the transmembrane helix S6, which flanks the selectivity filter.

Apart from the C-type inactivation, another characteristic feature of the $hK_v1.3$ channel distinguishes it from other voltage-gated potassium channels: high sensitivity to scorpion peptide toxins,¹⁸ such as margatoxin (MgTX) and charybdotoxin (CTX). Similar to other members of the scorpion toxin family, these two toxins act on potassium channels with a 1:1 stoichiometry^{21,22} and high affinity.²¹ The MgTX and CTX are similar in size (37 and 39 amino acids, respectively), and both adopt a fold structure named cysteine-stabilized alpha/beta motif (CSαβ). The secondary structure of these peptides consists of two or three β-strands and one α-helix and is stabilized by three disulfide bonds.²³ The key residue for blocking the ion flux through the channel (K27 in CTX and K28 in MgTX) lies within one of the β-sheets.^{24,25} Other important functional residues of both CTX and MgTX are located on the flat surface of the β-sheet. In addition, S10, K11 in CTX and K11, K18 in MgTX, which have strong electrostatic interactions with K^+ channels, are placed in the α-helix.^{25–29}

It has been reported that most scorpion toxins share a functional dyad. This functional dyad is composed of a basic

Received: October 25, 2011

Revised: March 15, 2012

Published: April 10, 2012

lysine (K27 in CTX and K28 in MgTX) protruding into the channel pore and a hydrophobic residue (Y or F) interacting with channel residues to stabilize the toxin–channel binding. These critical residues of the functional dyad are located in the β -sheet of the toxin. The key residues K27 in CTX and K28 in MgTX likely protrude into the channel pore, thereby preventing K^+ flux. In CTX, mutation of K27 reduces the toxin's binding affinity up to 300-fold.^{26,27,30,31} Several interacting pairs of residues between the toxin and the channel have been identified by mutational studies.^{32–35} Mutational data, in combination with molecular dynamics simulations, revealed that the *hK_v1.3* channel residues G375, T373, S374, D397, D381, and H399 in the outer pore area and Y395 in the selectivity filter are important in formation of the toxin–*hK_v1.3* channel complex.^{25,36}

Although three-dimensional (3D) structures of most scorpion toxins are highly similar to each other, important details of molecular interactions between different scorpion toxins and ion channels vary. In the present study, we investigated the behavior of the *hK_v1.3* wild-type and *hK_v1.3_H399N* mutant channels in the presence of the CTX and MgTX. We used the patch-clamp technique to observe the channel behavior. We employed molecular dynamics simulations to interpret the experimental data in terms of molecular structure. Early studies on C-type inactivation mechanism in *mK_v1.3* channels showed that residue 404 (equivalent to 399 in *hK_v1.3*) in the pore region is critical in the slow inactivation process,³⁷ with N at this position inducing the fastest C-type inactivation. Therefore we used in the current study the H399N mutant to maximally speed up C-type inactivation and to see whether these changes in C-type inactivation also change scorpion toxin–*hK_v1.3* interactions.

MATERIALS AND METHODS

Molecular Models and Molecular Dynamics Simulations. A model of the S4/S5/S6 region of the *hK_v1.3* potassium channel (S4/S5/S6) was built using the Yasara software,³⁸ by in silico mutation of a *mK_v1.3* potassium channel model (reported by Khabiri et al. (2011)³⁶), in turn based on the *K_v1.2* crystal structure (PDB entry: 2A79). Within the modeled region, the *hK_v1.3* displays 99% sequence identity with *hK_v1.2*, differing only in two amino acids (Ser vs Thr and Asn vs Ser) in the turret region. The *hK_v1.3* model was inserted into a pre-equilibrated palmitoyloleoylphosphatidylcholine (POPC) bilayer using a protocol (based on INFLATEGRO³⁹) described earlier.³⁸ Afterward, a copy of the model was modified by introducing a H399N mutation in all four monomers, using the Yasara software.³⁸ A single protonation state for this histidine was assumed, with the proton located on atom NE2 in the histidine ring. We used the published CTX and MgTX structures, determined experimentally by NMR spectroscopy (PDB ID 2CRD and 1MTX for CTX and MgTX, respectively), for molecular modeling experiments. Docking of the CTX and MgTX structures to the *hK_v1.3* model was performed as described earlier³⁶ using the AutoDock 4.0⁴⁰ module implemented in Yasara.³⁸

Simulations were performed with the GROMACS 4.0.7 software suite^{41,42} employing the OPLS all-atom force field⁴³ adapted for POPC lipids based on parameters of Berger et al. (1997)⁴⁴ and Marrink et al. (1998).⁴⁵ The wild-type and mutant *hK_v1.3*, as well as the CTX–*hK_v1.3* and MgTX–*hK_v1.3* complexes, were solvated by water molecules described by the extended simple point charge model of water.⁴⁶ Counter-

ions were added to achieve electric neutrality. Molecular dynamics simulations were carried out in the isothermal–isobaric (NPT) ensemble employing a 2 fs time step. Periodic boundary conditions were used. Initial velocities were assigned by applying a Maxwell distribution at 300 K. Lennard-Jones and electrostatic interactions were cut off at a distance of 10.0 Å, and the long-range electrostatic interactions were computed employing the particle-mesh Ewald method.⁴⁷ The temperature was kept at 300 K by separately coupling the protein and solvent to an external temperature bath ($T = 0.1$ ps). The pressure was kept constant at 1 bar by weak coupling ($T = 2.0$ ps) to a pressure bath using the Parrinello–Rahman algorithm,⁴⁸ which was employed with a semi-isotropic mode. The temperature coupling was achieved using the Nose–Hoover⁴⁹ algorithm. The SETTLE and SHAKE⁵⁰ (nonwater) algorithms were used to constrain covalent bond lengths in water and nonwater parts of the system, respectively. All data analysis was done using GROMACS utilities.

Molecular Biology. The *hK_v1.3* wild-type plasmid was a generous gift by Prof. Dr. O. Pongs (Institut für Neurol Signalverarbeitung, Zentrum für Molekulare Neurobiologie, Hamburg, Germany). It contains the human *K_v1.3* gene in a pRc/CMV vector (Invitrogen, Carlsbad, CA) with a CMV promoter for protein expression in mammalian cells. The *hK_v1.3_H399N* mutant channel gene was generated from the wild-type construct using the quick-change site-directed mutagenesis kit (Stratagene, Amsterdam, Netherlands).

Cells. Cell culture experiments were performed in COS-7 cells, obtained from the Deutsche Sammlung von Mikroorganismen und Zellkulturen GmbH (DSMZ, Braunschweig, Germany; No. ACC 60). The cells were maintained in Dulbecco's modified Eagle's medium with high glucose (Invitrogen, Carlsbad, CA) containing 10% fetal calf serum (PAA Laboratories GmbH, Coelbe, Germany) cultured at 37 °C and 10% $p(CO_2)$.

Transfection. For transient transfection of COS-7 cells, we used the Fugene 6 transfection reagent (Roche Molecular Biochemicals, Mannheim, Germany). Cells were grown to ~80% confluence and cotransfected with 3–5 μ g of the appropriate channel DNA and 1.5 μ g of GFP (green fluorescent protein) DNA (BD Biosciences Clontech, Palo Alto, CA).

Chemicals and Solutions. All measurements were carried out in an external bath solution containing 160 mM N-methyl-D-glucamine (NMDG), 2 mM CaCl₂, 1 mM MgCl₂, 4.5 mM KCl, and 5 mM HEPES. The osmolarity was 290–320 mOsm, and the pH was adjusted to 7.4 with HCl. The internal pipet solution [KF]_i contained 155 mM KF, 2 mM MgCl₂, 10 mM EGTA, and 10 mM HEPES. The osmolarity was 290–320 mOsm, and the pH was adjusted to 7.2 with KOH. All lyophilized samples of CTX and MgTX (Latoxan, Valence, France; Bachem, Bubendorf, Switzerland) were kept at –20 °C, and final dilutions in the external bath solutions containing 0.1% bovine serum albumin (Sigma-Aldrich Chemie, Steinheim, Germany) were prepared prior to measurements.

Electrophysiology. All experiments were carried out by using the whole-cell recording mode of the patch-clamp technique¹⁷ at room temperature (18–22 °C). Bath solutions in the recording chamber were exchanged by a simple syringe-driven perfusion system. Electrodes were pulled from glass capillaries (Science Products, Hofheim, Germany) in three stages and fire polished to resistance of 2–4 M Ω , as measured in the bath. Membrane currents were measured by an EPC-9

patch clamp amplifier (HEKA Electronik, Lambrecht, Germany) interfaced to a PC running acquisition and analysis software (Patchmaster/Fitmaster v2.00). All current recordings were filtered by a 2.9-kHz Bessel filter and recorded with a sampling frequency of 1–5 kHz. Series resistance compensation (75–80%) was used if the current exceeded 2 nA. Capacitative and leak currents were subtracted using the P/10 procedure. Current decays were fitted by a single exponential function, $I_{(t)} = A^* \exp(t/\tau_{in})$, with τ_{in} being the inactivation time constant.

RESULTS AND DISCUSSION

Influence of the H399N Mutation on $hK_v1.3$ Channel Behavior. In order to investigate the effect of CTX and MgTx on current through wild-type and mutant $hK_v1.3$ channels, we initially characterized the current flowing through the wild-type and $hK_v1.3$ _H399N mutant channels in the absence of toxins (Figure 1). Whole cell currents were elicited by depolarizing

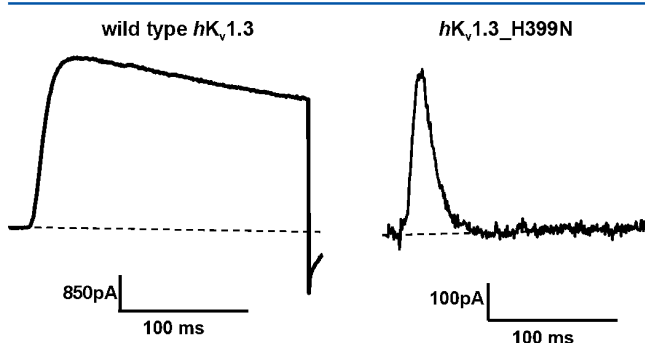


Figure 1. Current through $hK_v1.3$ wild-type and $hK_v1.3$ _H399N mutant channels. Whole cell currents were elicited by 200 ms depolarizing voltage steps to +40 mV from a holding potential of -120 mV.

voltage steps to +40 mV from a holding potential of -120 mV every 30 s in a bath solution containing 4.5 mM KCl. The pulse duration was 200 ms for wild-type and mutant channels. During a depolarizing pulse, after reaching a peak, the K^+ currents through the wild-type channels exhibit an exponential decay. The time course of this C-type inactivation can be estimated by fitting the current decay by a single exponential function. Our measurements show that the inactivation time constant (τ_{in}) of $hK_v1.3$ wild-type channel is 450 ± 55 ms ($n = 5$). The H399N mutant inactivates much faster, with the inactivation time constant of 8 ± 1 ms ($n = 10$). In order to obtain a molecular explanation of why the H399N mutant channels exhibit a much faster C-type inactivation than wild-type channels, we performed MD simulations. To avoid disturbances to channel's homotetrameric structure, known to occur^{51,52} in the absence of potassium ions, three potassium ions interleaved with water molecules were inserted in the potassium channel model as described before.^{36,53–55}

Figure 2A shows that the root-mean-square deviations (rmsd) of the $C\alpha$ atoms of the $hK_v1.3$ wild-type and $hK_v1.3$ _H399N mutant channels reached a plateau after ~10 and ~25 ns, respectively. For the WT channel, the equilibrated structure was stable and maintained its conformation and symmetry from that point on, while the mutant structure was still slightly drifting. The lower stability of the mutant protein model can be explained by an observed interruption of the interaction network beneath the selectivity filter (SF), affecting interactions both within and between the individual subunits. The continuous increase of the rmsd during the first 25 ns of the MD simulations is related to the instability of the selectivity filter and changes in the turret related to the orientation of N399. After 25 ns, once N399 finds its new stable conformation, the rmsd value reaches a plateau. To explore the dynamic behavior of the channels and their individual amino acids, we measured the root-mean-square fluctuation (rmsf) for the equilibrated phase of the simulations (Figure

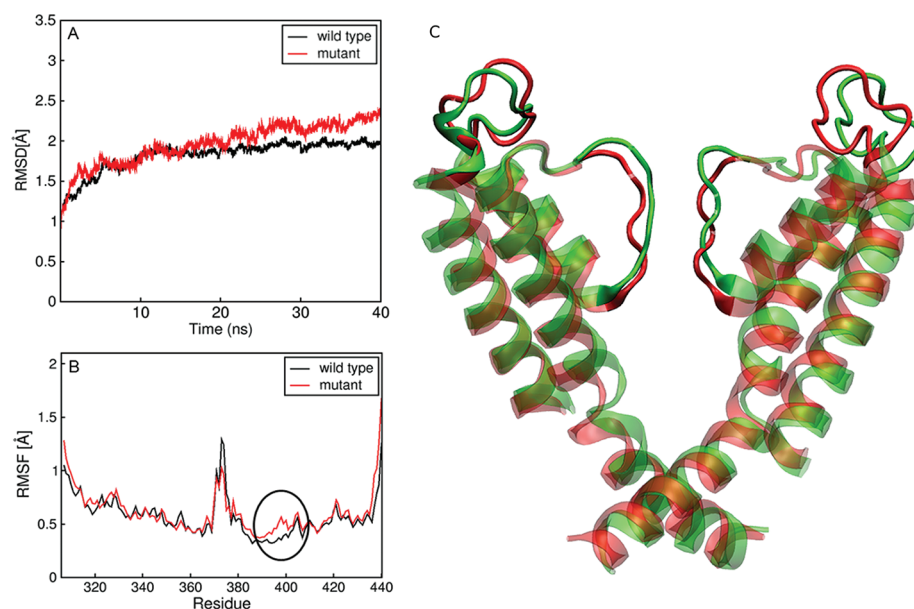


Figure 2. rmsd of $hK_v1.3$ wild-type and $hK_v1.3$ _H399N mutant channels (A). Comparison of the average rmsf of $hK_v1.3$ wild-type and mutant channels in the absence of toxins (B). The circle marks the selectivity filter (SF) region. Conformational differences of the turret and the selectivity filter between $hK_v1.3$ wild-type and $hK_v1.3$ _H399N mutant channels (C). The $hK_v1.3$ wild-type channel is shown in red, the $hK_v1.3$ _H399N mutant channel in green.

2B). Amino acids close to the point mutation, i.e., within the upper part of the selectivity filter, showed larger rms fluctuations in comparison with the wild-type, demonstrating a higher flexibility in the upper part of the selectivity filter, especially at position D397. Our molecular dynamics simulations raise the possibility that there is a relationship between flexibility of the selectivity filter and the current decay time course: higher flexibility of the selectivity filter might underlie the observed faster current decay during depolarization in the mutant channel.

In a bacterial potassium channel (*KcsA*), an important role in K⁺ channel inactivation is played by the amino acid network behind the selectivity filter.^{56–58} Within this network, the residue D80 is key, with the strongest effect on C-type inactivation. The corresponding residue in the *hKv1.3* channel is D397. Other known important residues of the *hKv1.3* network are H399 and W384. Mutations of each of these amino acids might alter the network, potentially allowing insights into the functional mechanism and structural requirements of C-type inactivation. Mutations of residues D397 and W384 result in channels with no measurable currents^{59–62} and are thus of limited interest. Therefore we introduced a mutation in the third key position, H399, and investigated its effect on the *hKv1.3* channel function.

The MD trajectory of the point mutation revealed a significant conformational change in the amino acid network (compare Figure 3A and B). In the wild-type channel, histidine 399 does not participate in direct electrostatic interactions with the adjacent monomers. Unlike histidine, asparagine contains

both a carbonyl and an amide group on the side chain. Since the asparagine amide group can accept and donate two hydrogen bonds, this amino acid has a high disposition to form hydrogen bonds with adjacent groups. Our MD simulations indeed reveal the presence of electrostatic interactions between N399 and other residues. Interestingly, the residue to contribute the strongest hydrogen bond with the N399 residue is D397 of the adjacent monomer. The amide group of N399 competes for the D397 carboxylic group with the indole group of W384. Because of higher propensity of the N399 amide group to form hydrogen bonds than that of the indole amine group of W384, N399 dominates the competition. As D397 loses its interaction with W384, it reorients toward the solution to form a salt bridge with the amide group of N399 on the protein surface (Figure 3B). In order for the W384 indole group to create the new hydrogen bond with the N399 carbonyl group, W384 undergoes a reorientation. As a consequence of this conformational change, the key stabilizing interaction between D397 and the W384 indole group behind the selectivity filter is broken, and the selectivity filter becomes more flexible (Figure 2B).

The flexibility of the turret is also altered. In *hKv1.3* wild-type channels (Figure 3A, right), E368 belonging to the turret has electrostatic interactions with the backbone amine groups of V401 and T402. In the H399N mutant (Figure 3B, right), E368 has a trifurcated interaction with S376 in the turret, and with V401 and T402 in the pore region. In contrast to the selectivity filter, H399N mutation stabilizes the turret region. Losing the structure and stability in the selectivity filter region, however, might cause the *hKv1.3_H399N* channel to inactivate very fast during depolarizations either through the conformational change itself or through the altered rigidity–flexibility of the selectivity filter.

Interactions of CTX and CTX with *hKv1.3* Wild-Type and *hKv1.3_H399N* Mutant Channels. Both CTX and MgTX abolish most of the current through the *hKv1.3* channels, even at low (10 nM) concentrations (Figure 4). In contrast, the two toxins differed in their effect on the H399N mutant channel. Specifically, CTX did not affect the peak current through *hKv1.3_H399N* mutant channels even at 100 nM, while MgTX at the same concentration did reduce this

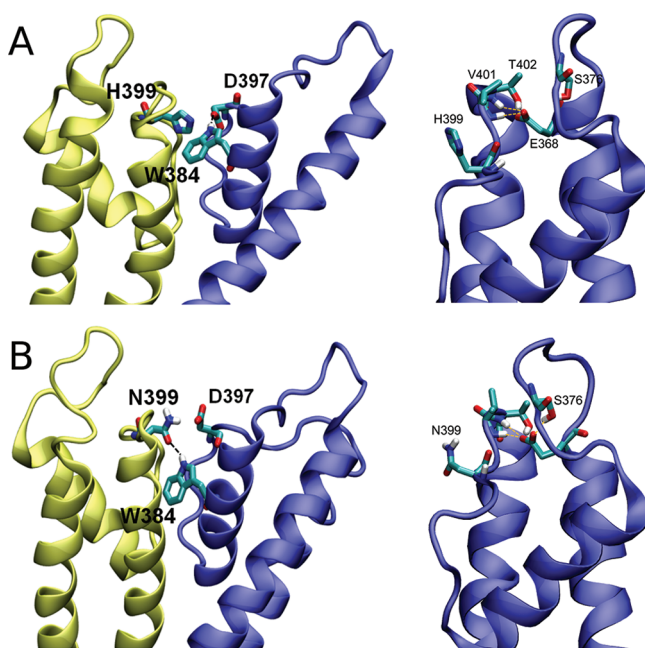


Figure 3. Amino acid network behind the selectivity filter in wild-type (A, left) and the distortion of this network by the H399N substitution (B, left). For clarity we only show S6 and part of S5 of monomer A (blue) and monomer D (yellow). In both panels the right side focuses on important residues in the turret; in *hKv1.3* wild-type channels (A, right), E368 belonging to the turret has electrostatic interactions with the backbone amine group of V401 and T402. In *hKv1.3_H399N* channels (B, right), E368 has a trifurcated interaction with S376 in the turret and V401 and T402 in the pore region. This network of interactions stabilizes the turret region.

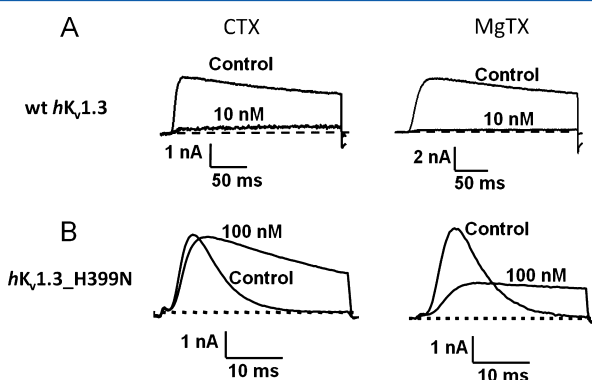


Figure 4. Effect of CTX (left) and MgTX (right) on current through *hKv1.3* wild-type (A) and *hKv1.3_H399N* mutant (B) channels. Representative whole cell currents were elicited by depolarizing voltage steps to +40 mV from a holding potential of -120 mV in the absence and presence of CTX (left) and MgTX (right). The voltage step was 200 ms for the wild-type (A) and 50 ms for the H399N mutant (B) channels.

current. Both CTX and MgTX, however, slowed down the rate of H399N mutant inactivation, by a factor of ~ 5 and ~ 12 , respectively.

In order to gain a molecular understanding of the effect of CTX and MgTX on *hK_v1.3* wild-type and *hK_v1.3_H399N* mutant channels, we performed molecular dynamics simulations.

Both CTX and MgTX were placed manually close to the equilibrated *hK_v1.3* wild-type channel structure and docked as described previously,^{25,36} while K27 in CTX and K28 in MgTX faced toward the selectivity filter. During the simulations, the rmsd of both the channel molecules (Figure 5A) and toxins

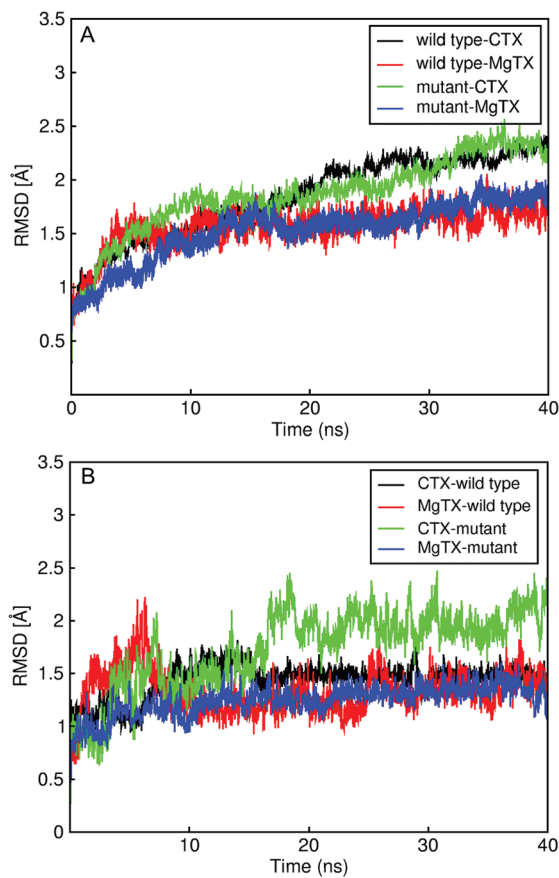


Figure 5. rmsd of *hK_v1.3* wild-type and *hK_v1.3_H399N* mutant channels in the presence of MgTX and CTX (A) and rmsd of the two toxins, MgTX and CTX, while they bind to the channels (B).

(Figure 5B) reached reasonable stability. Both toxins maintained the same distance from the channels, as determined by measuring the distance between the centers of mass of the toxin and *hK_v1.3* channel molecules (Figure 6).

Table 1 shows the interacting amino acids of MgTX and CTX with the *hK_v1.3* wild-type channel. K27 in CTX and K28 in MgTX appear to be the key residues blocking the pore. The result for the CTX interacting residues is consistent with previous studies.^{25,36} K27 in CTX and K28 in MgTX interacted symmetrically with Y395 from all four monomers of the *hK_v1.3* wild-type channel. In both toxins, this key residue is located in the middle of the second β -strand. Residues T8 and P10 in the turn between the first β -strand and the α -helix of MgTX interacted with T373 and D397 located in the turret and the selectivity filter of the *hK_v1.3* wild-type channel. These interactions were missing in the CTX–*hK_v1.3* complex. The

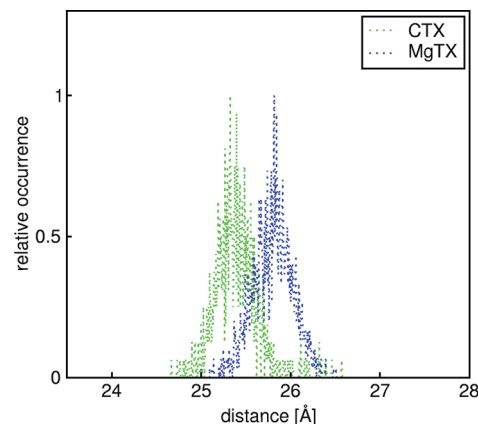


Figure 6. Distance of toxins from the *hK_v1.3* channel. The histogram shows the distribution for both toxins in the course of the simulation measured as the distance of the center of mass of the toxins from the center of mass of the channel tetramer. The relative occurrence values are normalized in order to get a unit value for the most probable distance. The histogram shows that both toxins are in a similar distance from the channel on average, 25.3 and 25.8 Å, respectively.

Table 1. Major Interactions between Pairs of Amino Acid Residues of CTX and *hK_v1.3_H399N* Mutant (Left) and Major Interacting Residues between MgTX and *hK_v1.3* Wild-Type and *hK_v1.3_H399N* Mutant (Right)

CTX	<i>hK_v1.3</i>	<i>hK_v1.3_H399N</i>
F2	T373(A)	T373(D)
K11	S374 (D)	
H21	G375(D)	
N22	P372(B)	
T23	G375(C)	
R25	D397, D381(A)	
K27	Y395(A, B, C, D)	D397(A)
M29	H393(D)	G396(D), D397(A)
N30	T373(D)	D397(D)
K31	D397(A)	D397(A)
R34	T373(A)	
Y36	D381(C)	V401(A)
S37	K406(A)	N399(A)
MgTX	<i>hK_v1.3</i>	<i>hK_v1.3_H399N</i>
T1		G375(A)
N4		T373(D), D381(D)
T8	T373(D), V401(D)	
P10	D397(D)	
K11	D381(D)	
K18	T373(B)	
Q20		S374(A), T373(A)
F21		T373(A)
S24	S374(B), G375(B)	
G26	D397(B)	
K28	Y395(A, B, C, D)	D397(B)
C29	D397(A)	
M30	D397(C)	
N31	H399(A)	G375(B), V401(B)
K33		D397(D)
K35	D397(C)	D397(A)
Y36	G396(C)	D397(C)
P38	T373(C)	
H39	D381(B)	

most significant interactions between MgTX and the *hK_v1.3* channel are related to D397. Five residues in MgTX, P10, G26, C29, M30, and K35 are interacting with D397 from all four monomers, while in CTX only R25 has an interaction with D397. When comparing the minimum distance of the center of mass of each residue in MgTX and CTX to the *hK_v1.3* wild-type channel, in the case of MgTX more amino acid residues seem to interact with the *hK_v1.3* channel (Figure 7A and B,

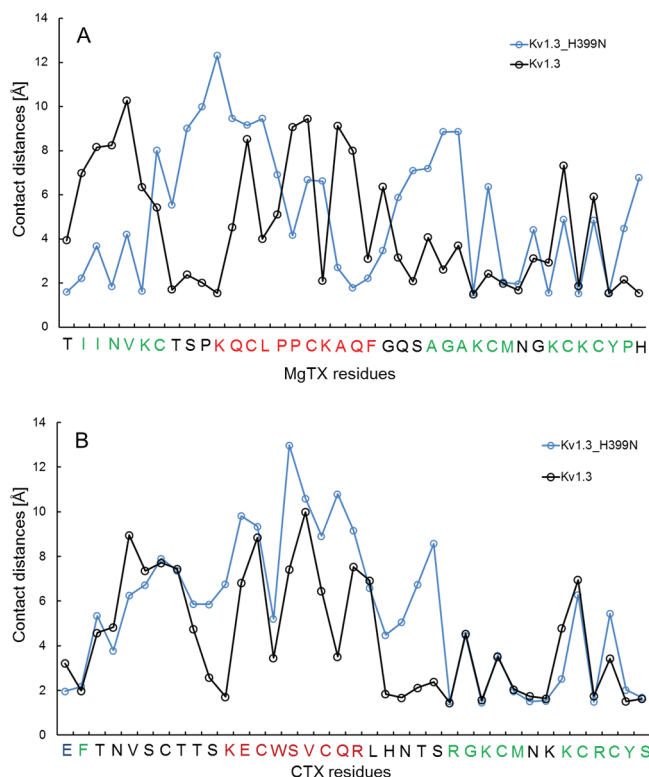


Figure 7. Minimum distance of MgTX (A) and CTX (B) residues to the *hK_v1.3* and the *hK_v1.3_H399N* channels. The measured distances are the average minimum distances between the center of mass of each individual toxin residue and the closest channel residue. The colors indicate the following: green, β -strand; black, β -turn; red, α -helix; Cys residues participating in S-S bridges in the toxin structure are highlighted yellow.

black graph). Despite having a very similar fold, CTX and MgTX show only 45% sequence identity in a primary sequence alignment of the two sequences (Figure 8). The larger number

CTX	-EFTNVSC TT S KE CWSV C QRLHNTS R G-KCMNK K C R Y S --	37
MgTX	-T I I N V K C T S P K O C L P P C K A Q F G Q S A G A K C M N G K K C Y P H --	39

Figure 8. Primary sequence alignment of CTX and MgTX. Green, β -strand; black, turns; red, α -helix; yellow highlight; Cys residues participating in S-S bridges in the toxin structure are highlighted yellow.

of interactions together with an extra positive charge in the case of MgTX might result in a higher affinity, represented by the higher binding energy calculated from the force field of -86.7 kcal/mol for MgTX compared to -72 kcal/mol for CTX. In both cases the binding energy was calculated for the final equilibrated complexes, considering the internal energy obtained with the Amber99 force field, as well as the electrostatic and van der Waals solvation energy. Hereby, the

electrostatic solvation energy estimates the interaction energy between the solvent and the solute by treating the solvent as a continuum without explicit solvent molecules. A first-order boundary element approximation to the solvation energy was used. van der Waals solvation energy was calculated as a function of the solute's solvent accessible surface area. The entropic cost of fixing the ligand in the binding site is almost impossible to calculate accurately, but fortunately not needed since it mainly depends on characteristics that are constant during the simulation (ligand and protein size, side chains on the surface, etc.). The entropic component is thus a constant factor that can be omitted. The more negative the binding energy, the more favorable the interaction in the context of the chosen force field. As mentioned before, in both toxins, CTX and MgTX, the β -sheet is a part of the contact surface, when K27 and K28, respectively, occlude the selectivity filter. Although the initial docked conformation of both toxins is practically identical with respect to the pore and the turret regions, we can observe differences in the dynamical behavior and three-dimensional structure of the toxins after 40 ns of unrestrained molecular dynamics simulation. Both toxins are small, flexible peptides with a three-dimensional structure that has only a weak hydrophobic core, and therefore the structure strongly depends on its environment. Figures 9A and B show the resulting conformation of CTX and MgTX after 40 ns of MD when both are blocking the wild-type channel entirely. The helix, which is important for toxin channel interaction³⁵ and determines the direction of the dipole moment from the α -helical region to the β -sheet, is different in each toxin. While the

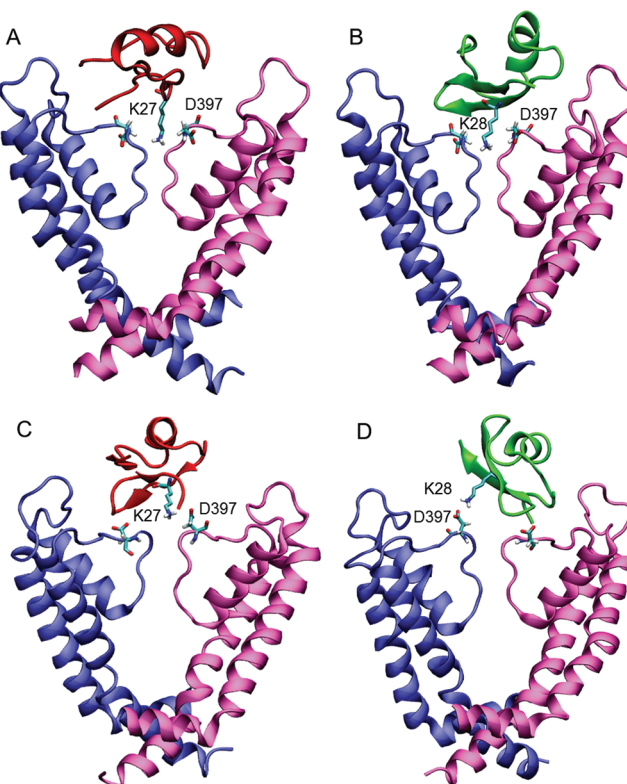


Figure 9. Interaction of CTX (A) and MgTX (B) with *hK_v1.3* wild-type and interaction of CTX (C) and MgTX (D) with the *hK_v1.3_H399N* mutant channel. K27 in CTX, K28 in MgTX and D397 are shown in licorice representation. For clarity, only monomers A (blue) and B (magenta) are shown; helix S4 was deleted.

helix in CTX lies more horizontally relative to the channel surface, the helix in MgTX seems to be more tilted. In order to quantify the difference between the two helices, we calculated the angle of each helix axis relative to the x -axis with the x -axis defined as the axis which is parallel to the surface of membrane. The mean angle for the helix axis in CTX is $\sim 14^\circ$ and $\sim 56^\circ$ in MgTX (Figure 10), thus resulting in an angle of 42° between

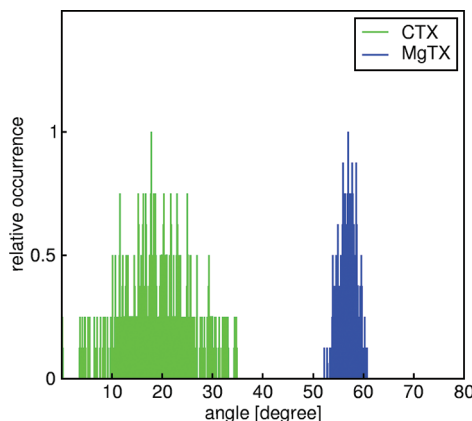


Figure 10. Angle of CTX and MgTX helix relative to the membrane surface. First the helix axis is defined. Then the angle was calculated between the helix and the z -axis (which is the axis perpendicular to the surface of membrane) by g_sgangle in Gromacs. The measured angle was subtracted by 90 to get the angle between the helix and the membrane surface (x -axis). The relative occurrence values are normalized in order to get a unit value for the most probable angle. The histogram shows, on average, that the axis of the helix in CTX is $\sim 14^\circ$ while in MgTX it is $\sim 56^\circ$.

CTX and MgTX. During the last 10 ns of simulation, we can observe a broader angle distribution in CTX in comparison to MgTX, which might be related to the weaker binding of CTX compared to MgTX.

Molecular dynamics simulations of the $hK_v1.3_H399N$ mutant channel with bound CTX or MgTX reveal why these two toxins were not able to fully block current through the mutant channel in the electrophysiological experiments. Panels C and D of Figure 9 show the final position of CTX and MgTX after 40 ns simulation. In sharp contrast to wild-type, both toxins seem to sit differently tilted on the mutant channel surface. Key residues K27 in CTX and K28 in MgTX are trapped by D397 on the protein surface in the upper part of the selectivity filter. As described before, D397 in the mutant channel moved into a different position away from the pore during the molecular dynamics simulation, with its carboxyl group now oriented toward the solvent and too far from being able to coordinate the amino group of K27 (or K28) in a concerted way. Thus the whole system gets asymmetric, with lysine interacting with D397 from one monomer only, while in wild-type D397 is an integral part of the pore and K27 (or K28) interacted with D397 from all four monomers. In the mutant channel this lysine residue is situated off-center in both toxins as can be quantified by measuring the distances of MgTX–K28 and CTX–K27 from Y395 in all four monomers of wild-type (Figure 11A) and mutant channels (Figure 11B). The distance between K28 in MgTX and Y395 in monomer D of the mutant channel is smaller than the distance from the three other Y395 residues in monomers A–C. K27 in the CTX- $hK_v1.3_H399N$ complex has a closer contact with Y395 in monomer C compared with the three other monomers. The minimum

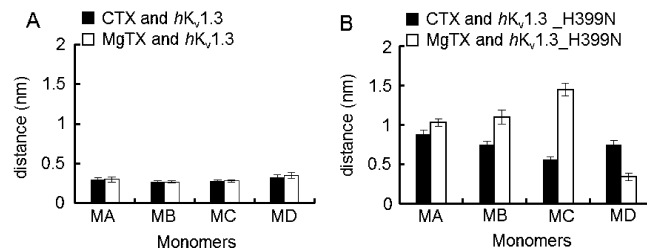


Figure 11. Distance between the center of mass of the key lysine residue of CTX or MgTX and the center of mass of Y395 in all four monomers (MA, MB, MC, MD) of the $hK_v1.3$ wild-type and the $hK_v1.3_H399N$ mutant channels (in nm). Filled columns give the distance between K27 of CTX and Tyr395 in all four monomers (MA, MB, MC, MD) of the $hK_v1.3$ wild-type (A) and the $hK_v1.3_H399N$ mutant (B) channels. Open columns give the distance between K28 of MgTX and Y395 in all four monomers (MA, MB, MC, MD) of the $hK_v1.3$ wild-type (A) and the $hK_v1.3_H399N$ mutant (B) channels.

distances of MgTX (Figure 7A) and CTX (Figure 7B) from $hK_v1.3$ and $hK_v1.3_H399N$ reveal that the number of residues close to the channel is higher for MgTX than for CTX and that both toxins have different orientations. The distances of some of these residues in the MgTX- $hK_v1.3_H399N$ complex are shorter than the distances of the same residues in the MgTX- $hK_v1.3$ complex. Residues 1–6 (TIINV) in the first β -strand in the extended N-terminal and residues 16, 19, and 20 (P, A, and Q) in the C-terminal of the α -helix from MgTX are closer to the $hK_v1.3_H399N$ mutant than to the $hK_v1.3$ wild-type channel. On the other hand, the amino acid sequence SP located in the turn between the first β -strand and the α -helix and KQ located in the α -helix, the SAGA sequence, C29 in the second β -strand, and residues P and H in the third β -strand are further from the $hK_v1.3_H399N$ mutant channel than from the $hK_v1.3$ wild-type channel. Hereby, CTX is behaving similar to MgTX (Figure 7B). As reported before³⁶ and also shown in Figure 7B, there are 14 major interactions between CTX and the wild-type channel whereas in the CTX- $hK_v1.3_H399N$ complex we can observe only 10 interactions.

These results are consistent with the higher ability of MgTX to block the mutant channel in the present experimental results when compared to CTX. Table 1 shows major interactions of both toxins with the $hK_v1.3_H399N$ mutant channel. Main differences of the mutant channel from wild-type include the lack of interactions of pore occluding K28 in MgTX with Y395 in the four monomers and the formation of a new contact between K28 and D397 in monomer B. It seems that the lack of pore occluding interactions and the tilting of MgTX at the same time cause the passage of K^+ ions through the mutant channel. In addition, it looks as if the binding of toxins to the mutant channels changed the inactivation time course. Figure 12 shows the root-mean-square fluctuation (rmsf) of the backbone $C\alpha$ atoms of the mutant channels in the presence and absence of toxins. The rmsf of $C\alpha$ atoms in the mutant channel implies a different degree of flexibility in the selectivity filter region in the presence and absence of toxins. Binding of CTX or MgTX to the mutant channel reduces fluctuations and contributes to a stabilization in the selectivity filter and might thereby prevent the structural rearrangements associated with fast C-type inactivation in the mutant $hK_v1.3_H399N$ channel. Experimental results in combination with molecular dynamics simulations data showed that there is a correlation between the C-type inactivation rate and the level of structural stability in the outer part of the selectivity filter of $hK_v1.3$. This structural

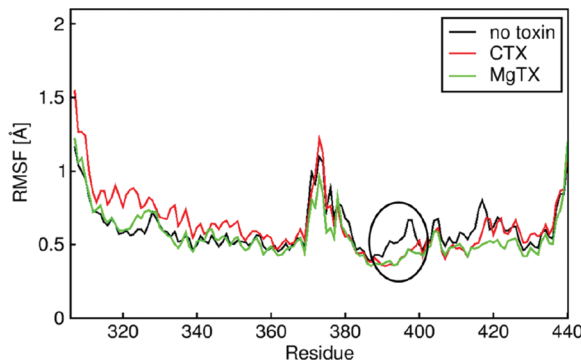


Figure 12. Average rms fluctuations of the individual residues in the *hK_v1.3_H399N* channel in the presence and absence of toxins. The circle marks the SF region.

stability originated from the interaction between two residues, W384 in the pore helix and D397 in the outer part of the selectivity filter. It seems that this connection between the pore helix and the selectivity filter conferred a special degree of stability to the selectivity filter and the outer vestibule of *hK_v1.3* channels. These findings are similar to the sodium and calcium channel model proposed by Tikhonov and Zhorov (2011), in which conserved residues around the selectivity filter of sodium and calcium channels have several intra- and interdomain contacts that support structural stability of the outer pore of these channels.⁶³ Although mutations produced a more flexible area in the upper part of the selectivity filter, at the same time the turret region of the mutant channels was stabilized, suggesting structural changes in the outer pore of the mutant channels. Previous studies on sodium and calcium channels showed that binding of tetrodotoxin (TTX) to sodium channels stabilized the ascending limbs of the sodium channel.⁶³ Since our mutation changed the network of interactions behind the selectivity filter and in the turret region, it seems reasonable to expect altered or novel contacts between toxins and mutant channels. These novel contacts could stabilize the upper part of the selectivity filter in the mutant channels. In contrast to the toxin-free mutant channel, the high stability of the outer pore and the selectivity filter in the toxin-bound mutant channel could prevent and/or slow down the structural rearrangements in the outer mouth of the H399N mutant channel associated with its fast inactivation.

CONCLUSION

CTX and MgTX block current through *hK_v1.3* wild-type channels, but the affinity of both toxins toward the *hK_v1.3_H399N* mutant channels is clearly reduced. Even 100 nM of CTX were unable to block current through the mutant channels. The same concentration of MgTX only partially blocked the current through the mutant channels, while a 10-fold smaller concentration of both toxins (10 nM) could totally abolish the current through the wild-type channels. Moreover, our experimental data show that the decay time for macroscopic K⁺ current through the *hK_v1.3_H399N* mutant channels is faster than in the case of the wild-type channel and application of both toxins slowed down the fast current decay of mutant channels. Finally, our data demonstrated that the asymmetric binding of CTX and MgTX to the mutant channels results in a loss of pore-occluding interactions, while some different and new interactions between toxins and mutant channels are established that reduce fluctuations in the network

behind the selectivity filter and contribute to a stabilization of the selectivity filter that might result in a change in C-type inactivation.

AUTHOR INFORMATION

Corresponding Author

*Tel. +49 731 500 23253; fax +49 731 50023260; e-mail stephan.grissmer@uni-ulm.de (S.G.); tel. +420386361297; fax +420386361279; e-mail ettrich@nh.cas.cz (R.E.).

Author Contributions

[†]These authors contributed equally to this work.

Notes

The authors declare no competing financial interest.

ACKNOWLEDGMENTS

M.K. and R.E. acknowledge support from the Czech Science Foundation, 203/08/0114, and the Academy of Sciences of the Czech Republic. S.G. and A.N. were supported by grants from the DFG (Gr 848/14-1). Additionally, M.K. was supported by the University of South Bohemia, grant GAJU 170/2010/P. Access to the META centrum computing facilities is highly appreciated. S.G. and A.N. thank Ms Katharina Ruff for her excellent technical assistance.

REFERENCES

- (1) Chandy, K. G. *Nature* **1991**, *352*, 26.
- (2) Wulff, H.; Knaus, H. G.; Pennington, M.; Chandy, K. G. *J. Immunol.* **2004**, *173*, 776–786.
- (3) Mackenzie, A. B.; Chirakkal, H.; North, R. A. *Am. J. Physiol. Lung Cell Mol. Physiol.* **2003**, *285*, 862–868.
- (4) Vicente, R.; Escalada, A.; Coma, M.; Fuster, G.; Sanchez-Tillo, E.; Lopez-Iglesias, C.; Soler, C.; Solsona, C.; Celada, A.; Felipe, A. *J. Biol. Chem.* **2003**, *278*, 46307–46320.
- (5) Schlichter, L. C.; Sakellaropoulos, G.; Ballyk, B.; Pennefather, P. S.; Phipps, D. J. *Glia* **1996**, *17*, 225–236.
- (6) Khanna, R.; Roy, L.; Zhu, X.; Schlichter, L. C. *Am. J. Physiol. Cell Physiol.* **2001**, *280*, C796–806.
- (7) Arkett, S. A.; Dixon, J.; Yang, J. N.; Sakai, D. D.; Minkin, C.; Sims, S. M. *Recept. Channels* **1994**, *2*, 281–293.
- (8) Maruyama, Y. *J. Physiol.* **1987**, *391*, 467–485.
- (9) Schmidt, K.; Eulitz, D.; Veh, R. W.; Kettenmann, H.; Kirchhoff, F. *Brain Res.* **1999**, *843*, 145–160.
- (10) Fadool, D. A.; Levitan, I. B. *J. Neurosci.* **1998**, *18*, 6126–6137.
- (11) Jiang, Y.; Lee, A.; Chen, J.; Ruta, V. M.; Cadene, B.; Chait, T.; MacKinnon, R. *Nature* **2003**, *423*, 33–41.
- (12) Doyle, D. A.; Morais Cabral, J.; Pfuetzner, R. A.; Kuo, A.; Gulbis, J. M.; Cohen, S. L.; Chait, B. T.; MacKinnon, R. *Science* **1998**, *280*, 69–77.
- (13) MacKinnon, R. *Nature* **1991**, *350*, 232–235.
- (14) Yellen, G. *Nature* **2002**, *419*, 35–42.
- (15) Bezanilla, F. *Physiol. Rev.* **2000**, *80*, 555–592.
- (16) Lee, S. Y.; Banerjee, A.; MacKinnon, R. *PLoS. Biol.* **2009**, *7*, 0676–0686.
- (17) Hamill, O. P.; Marty, A.; Neher, E.; Sakmann, B.; Sigworth, F. J. *Pflügers Archiv.—Eur. J. Physiol.* **1981**, *391*, 85–100.
- (18) Gutman, G. A.; Chandy, K. G.; Grissmer, S.; Lazdunski, M.; MacKinnon, D.; Pardo, L. A.; Robertson, G. A.; Rudy, B.; Sanguinetti, M. C.; Stühmer, W.; Wang, X. *Pharmacol. Rev.* **2005**, *57*, 473–508.
- (19) Liu, Y.; Jurman, M. E.; Yellen, G. *Neuron* **1996**, *16*, 859–867.
- (20) Bernèche, S.; Roux, B. *Structure* **2005**, *13*, 591–600.
- (21) Aiyar, J.; Withka, J. M.; Rizzi, J. P.; Singleton, D. H.; Andrews, G. C.; Lin, W.; Boyd, J.; Hanson, D. C.; Simon, M.; Dethlefs, B. *Neuron* **1995**, *15*, 1169–1181.
- (22) MacKinnon, R.; Miller, C. *J. Gen. Physiol.* **1988**, *91*, 335–349.
- (23) Cornet, B.; Bonmatin, J. M.; Hetru, C.; Hoffmann, J. A.; Ptak, M.; Vovelle, F. *Structure* **1995**, *3*, 435.

- (24) Goldstein, S. A. N.; Pheasant, D. J.; Miller, C. *Neuron* **1994**, *12*, 1377–88.
- (25) Yu, K.; Fu, W.; Liu, H.; Luo, X.; Chen, K. X.; Ding, J.; Shen, J.; Jiang, H. *Biophys. J.* **2004**, *86*, 3542–55.
- (26) Park, C. S.; Miller, C. *Biochemistry* **1992b**, *31*, 7749–7755.
- (27) Goldstein, S. A. N.; Miller, C. *Biophys. J.* **1993**, *63*, 1613–15.
- (28) Stampe, P.; Kolmakova-Partensky, L.; Miller, C. *Biophys. J.* **1992**, *62*, 8–9.
- (29) Stampe, P.; Kolmakova-Partensky, L.; Miller, C. *Biochemistry* **1994**, *33*, 443–50.
- (30) Dauplais, M.; Lecoq, A.; Song, J.; Cotton, J.; Jamin, N.; Gilquin, B.; Roumestand, C.; Vita, C.; de Medeiros, C. L. *J. Biol. Chem.* **1997**, *272*, 4302–4309.
- (31) Bednarek, M. A.; Bugianesi, R. M.; Leonard, R. J.; Felix, J. P. *Biochem. Biophys. Res. Commun.* **1994**, *198*, 619–625.
- (32) Hidalgo, P.; MacKinnon, R. *Science* **1995**, *268*, 307–310.
- (33) Naranjo, D.; Miller, C. *Neuron* **1996**, *16*, 123–130.
- (34) Schreiber, G.; Fersht, A. R. *J. Mol. Biol.* **1995**, *248*, 478–486.
- (35) Stocker, M.; Miller, C. *Proc. Natl. Acad. Sci. U.S.A.* **1994**, *91*, 9509–9513.
- (36) Khabiri, M.; Nikouee, A.; Cwiklik, L.; Grissmer, S.; Ettrich, R. *J. Phys. Chem. B* **2011**, *115*, 11490–11500.
- (37) Jäger, H.; Rauer, H.; Nguyen, A. N.; Aiyar, J.; Chandy, K. G.; Grissmer, S. *J. Physiol.* **1998**, *506*, 291–301.
- (38) Krieger, E.; Darden, T.; Nabuurs, S. B.; Finkelstein, A.; Vriend, G. *Proteins: Struct., Funct., Bioinf.* **2004**, *57*, 678–683.
- (39) Kandt, C.; Ash, W. L.; Tielemans, D. P. *Methods* **2007**, *41*, 475–488.
- (40) Morris, G. M.; Goodsell, D. S.; Halliday, R. S.; Huey, R.; Hart, W. E.; Belew, R. K.; Olson, A. J. *J. Comput. Chem.* **1998**, *19*, 1639–1662.
- (41) Berendsen, H. J. C.; van der Spoel, D.; van Drunen, R. *Comput. Phys. Commun.* **1995**, *91*, 43–56.
- (42) Lindahl, E.; Hess, B.; van der Spoel, D. *J. Mol. Modell.* **2001**, *7*, 306–317.
- (43) Jorgensen, W. L.; Maxwell, D. S.; Tirado-Rives, J. *J. Am. Chem. Soc.* **1996**, *118*, 11225–11236.
- (44) Berger, O.; Edholm, O.; Jahnig, F. *Biophys. J.* **1997**, *72*, 2002–2013.
- (45) Marrink, S. J.; Berger, O.; Tielemans, D. P.; Jahnig, F. *Biophys. J.* **1998**, *74*, 931–943.
- (46) Essmann, U.; Perera, L.; Berkowitz, M. L. *J. Chem. Phys.* **1995**, *103*, 8577–8592.
- (47) Berendsen, H. J. C.; Postma, J. P. M.; Vangunsteren, W. F.; Dinola, A.; Haak, J. R. *J. Chem. Phys.* **1984**, *81*, 3684–3690.
- (48) Parrinello, M.; Rahman, A. *J. Appl. Phys.* **1981**, *52*, 7182–7190.
- (49) Noé, S.; Klein, M. L. *Mol. Phys.* **1983**, *50*, 1055–1076.
- (50) Ryckaert, J. P.; Ciccotti, G.; Berendsen, H. J. C. *J. Comput. Phys.* **1997**, *23*, 327–341.
- (51) Capener, C. E.; Proks, P.; Ashcroft, F. M.; Sansom, M. S. *Biophys. J.* **2003**, *84*, 2345–2356.
- (52) Zhou, Y.; Morais-Cabral, J. H.; Kaufman, A.; MacKinnon, R. *Nature* **2001**, *414*, 43–48.
- (53) Bernèche, S.; Roux, B. *Biophys. J.* **2000**, *78*, 2900–2917.
- (54) Hellgren, M.; Sandberg, L.; Edholm, O. *Biophys. Chem.* **2006**, *120*, 1–9.
- (55) Jensen, M. Ø.; Borhani, D. W.; Lindorff-Larsen, K.; Maragakis, P.; Jogini, V.; Eastwood, M. P.; Dror, R. O.; Shaw, D. E. *Proc. Natl. Acad. Sci. U.S.A.* **2010**, *107*, 5833–5838.
- (56) Cordero-Morales, J. F.; Jogini, V.; Chakrapani, S.; Perozo, E. *Biophys. J.* **2011**, *100*, 2387–2393.
- (57) Cordero-Morales, J. F.; Jogini, V.; Lewis, A.; Vásquez, V.; Cortes, D. M.; Roux, B.; Perozo, E. *Nat. Struct. Mol. Biol.* **2007**, *14*, 1062–1069.
- (58) Cuello, L. G.; Jogini, V.; Perozo, E. *Nature* **2010**, *466*, 203–208.
- (59) Aiyar, J.; Rizzi, J. P.; Gutman, G. A.; Chandy, K. G. *J. Biol. Chem.* **1996**, *271*, 31013–31016.
- (60) Perozo, E.; MacKinnon, R.; Bezanilla, F.; Stefani, E. *Neuron* **1993**, *11*, 353–358.
- (61) Wang, Z.; Fedida, D. *Biophys. J.* **2001**, *81*, 2614–2627.
- (62) Xu, Y.; Ramu, Y.; Lu, Z. *Nature* **2008**, *451*, 826–829.
- (63) Tikhonov, D. B.; Zhorov, B. S. *J. Biol. Chem.* **2011**, *4*, 2998–3006.